Journal of Radiation and Nuclear Applications
An International Journal

http://dx.doi.org/10.18576/jrna/100106

Sustainable Gamma Radiation Shielding: Coconut Shell Ash Modified Concrete for Radiation Protection Applications

U. Rilwan [1,2], *M.A. Abdulazeez* [2], *I. Maina* [1,2], *O.W. Olasoji* [2], *Atef El-Taher* [3], *I.S. Adeshina* [4], *M.I. Sayyed* [5,6],

[1]Department of Physics, Faculty of Natural and Applied Sciences, Nigerian Army University, P.O. Box 1500 Biu, Borno State, Nigeria.

[2]Department of Physics, Abubakar Tafawa Balewa University, Bauchi, Bauchi State, Nigeria.

[3]Department of Physics, Faculty of Science, Al-Azhar University, Assuit 71452, Egypt

[4]Department of Energy and Material Science, Institut National de la Recherche Scientifique, Universite du Quebec, Canada.

[5]Department of Physics and Technical Sciences, Western Caspian University, Baku, Azerbaijan.

[6]Department of Physics, Faculty of Sciences, Isra University, Amman, Jordan.

Received: 21 Oct. 2024, Revised: 25 Nov. 2024, Accepted: 23 Dec. 2024.
Published online: 1 Jan 2025.

Abstract: The present work looked at the gamma-ray shielding ability of concrete with cement partially replaced by coconut shell ash (CSA). We produced four novel concretes which include 0%CC, 10%CC, 20%CC, and 30%CC, where CC stands for CSA percentage cement replacement. The samples were tested for economic and environmental assessment using a mathematical approach and radiation shielding performance using both experimental techniques (NaI detector with Co-60 and C-137 sources) and theoretical techniques (Phy-X). The report revealed that 0%CC had the superior LAC value (0.386 cm^{-1}) in the lower energy range (0.15 MeV), while at higher photon energy, 30%CC exhibited the least value of LAC (0.169 cm^{-1}). For the tested photon energy spectrum, the values of the mean free path (MFP) were within 2.591 cm for 0%CC and 5.917 cm for 30%CC. The results of the cost-effectiveness analysis revealed 90% MCS (material cost savings) for the entire fabricated samples and 50% WUE (waste utilization efficiency) for concrete 30%CC, which indicates a great reduction in the cost of production. A high level of agreement between theoretical and experimental findings with RD (relative deviation) ranged from 0.771% to 4.520%. The report of the study confirmed that at a lower energy range, the radiation shielding strength of our concretes is enhanced with the presence of CSA and also gives a cost and eco-friendly substitute for radiation protection applications. The study lamented the CSA potential in sustainable development via the reduction of waste and cost of material while ensuring sufficient gamma shielding performance.

Keywords: Radiography; radiotherapy; gamma radiation shielding (GRS); sustainable concrete; coconut shell ash (CSA); cement replacement; environmental sustainability; eco-friendly.

1 Introduction

In recent times these short wavelengths and higher frequency nature of radiations (gamma radiation) because of their high penetrating power, have been taken so seriously [1]. Radiation is the emission or transfer of energy in the forms of electromagnetic waves and particles through a free space such as air, vacuum, etc. Gamma radiation has been often talked about in countless research papers, especially concerning medicine as a primary form of ionizing energy that can pass through materials due to its release from an atomic nucleus. This featured imaging technique of PET for medical use is effective as well as such infiltration levels seen in cancer cells from within the tumor. When this occurs, it means, the surrounding tissue around the cancer cell is damaged and ensures an efficient infiltration [2]. More intensive forms of this radiation, however, are used in devices like gamma knife radiosurgery to kill cancerous tumors within humans. Nevertheless, at a time when it is increasingly being used in medical practice and research that investigates its usage proliferates, knowledge of the nature and impact of gamma radiation proves mandatory. As these technologies evolve,

*Corresponding author e-mail: rilwan.usman@naub.edu.ng

it is important to focus on ensuring gamma radiation can be safely and effectively handled to protect patients, healthcare workers as well as the environment against possible harm [3].

The health risks for humans exposed to high levels of gamma radiation are dire. Acute radiation syndrome can occur from experiencing fatigue, queasiness, and throwing up [4]. The more time one is exposed to this radiation, the odds of cancer also rise both in leukemia and other cancers [5]. Its ionizing nature can lead to cellular and DNA damage, which in turn manifests into biological or health effects that can, among other things weaken the immune system) making it harder for the body to get away from illnesses. Protecting public health and minimizing safety risks in areas with high radiation exposure is critical, which makes it important to understand how gamma rays must be shielded effectively [6].

Efficient defenses are required to reduce the harmful effects of gamma radiation. Radiation shielding materials are generally used to reduce or absorb the radiation, that could be harmful if such exposures were at a closer range [7]. Its efficiency is established by its parts, concentration, and thickness. If you are using gamma radiation, standards and regulations are examining the way the facility is shielded [8]. This is especially critical in countries that are still developing and have less emphasis on mechanisms to ensure radiation safety. In other words, a new radiation shield must be innovative, cost-effective, and green (eco-friendly) to improve the overall safety of using such materials [9].

Ceramics, lead, metal alloys, and glasses are some of the conventional materials that have shown promise as radiation shields. Since it is a very dense material and has high stopping power lead finds extensive use in shielding to reduce gamma radiation. Another great material for high-temperature applications is ceramics, especially as they are generally heat-resistant and possess very good mechanical strength. Metal alloys, often for the well-balanced properties of weight and strength, are also good at defense [10].

Because glass is a flexible material and looks elegant. Research indicates the importance of such substances in radiation safety with various uses as a helping hand to reduce exposure to these protons [11]. While effective, traditional shielding materials have some limitations. Although lead is great for insulation, it can also be dangerous and harmful to the environment if handled incorrectly. Ceramic materials may break under dynamic loads, so the bone may cause wear and structural problems [12]. While their high strength can make metal alloys ideal in some applications, they quickly become too expensive and heavy to be practical for others. Glasses, which can be tailored for the wearer, may not provide enough protection against high-energy gamma radiation unless they are made very thick and unwieldy [13]. These limitations highlight the need for novel engineered materials with strong shielding in addition to increased safety and sustainability [14].

Concrete has become a popular alternative to traditional radiation shielding materials. Both, its intrinsic properties in terms of accessibility, cost-effectiveness, and as functionalized one justifies it to be considered within shielding strategies [15]. Unlike ceramics or glass, concrete is malleable into large shapes that provide adequate protection while maintaining a low-burden load. Further, concrete can be modified to increase density and its radiation attenuation characteristics. It has been shown that concrete is very effective at blocking gamma radiation and also provides additional benefits such as fire protection, and strength, making concrete an ideal choice when it comes to shielding for any type of application [16].

For accuracy and validity in assessing gamma radiation shielding properties of concrete samples, it is essential to compare the theoretical (Phy-X) and experimental methods [17]. The real-world data are obtained from the experimental approach, while the theoretical predictions are obtained from the Phy-X calculations. Researchers can confirm the validity of the theoretical models, spot possible inconsistencies, and improve predictions by correlating the two approaches [18]. Additionally, this correlation makes it possible to evaluate the CSA effectiveness in improving gamma radiation shielding, determines mixed proportions, and guarantees that the concrete fulfills radiation protection requirements. Thus, the two approaches guarantee thorough comprehension and precise description of gamma radiation shielding with concrete [19].

Incorporating Coconut Shell Ash (CSA) into concrete mixes presents numerous economic and environmental benefits. If substituting traditional cement with CSA, the material costs can be reduced by approximately 30-40%, primarily due to the lower expenses associated with CSA production [20]. In addition, the replacement also altered the shielding effectiveness by 10-20%, mechanical strength by 5-15%, and the thermal conductivity reduces by 20-30%. This substitution does not only lead to financial savings but also significantly lowers the carbon footprint, achieving reductions of 60-70%. Such decreases are crucial in mitigating the negative impacts on the environment [21].

More so, concrete offers some extra structural protection against radiation. Coconut Shell Ash is an eco-friendly and natural material, which can able to improve the strength and density of concrete [22]. According to studies, the addition of coconut shell ash in concrete may lead to an alteration in radiation protection with a weight reduction [23]. This technique also helps to prevent waste by recycling agricultural waste products to support environmental sustainability [24]. The use of coconut shell ash in concrete is not only going to alter the capability for blocking radiation but also healthier as less harmful cement will be used resulting in lower exposure to silica dust and related health risks [25]. Furthermore, coconut shell ash is often less expensive than conventional cement offering an economic alternative for construction purposes and radiation shielding materials [26]. The current study intends to experimentally study the contribution of partial replacement of cement with coconut shell ash (CSA) on the γ-radiation shielding strength and cost-effectiveness of concretes. This is one of the major aims of the Sustainable Development Goals (SDGs), contributing immensely to a cleaner environment for hospital radiography and radiotherapy applications.

2 Experimental Section

2.1 Materials

The materials used in this research include coconut shells (CS), coconut shell ash (CSA), cement, sharp sand, granite, water, cylindrical plastic molds, and gamma-ray sources (Co-60 and Cs-137). A sodium iodide (NaI) detector, a lead collimator, and a Thermo-Scientific X-ray fluorescence analyzer (ARLQUANT'X-EDXRF) were also utilized for material characterization and gamma radiation shielding measurements.

2.2 Concrete Sample Fabrications

We collected the coconut shells (3 kg) from Keffi, Nasarawa State, washed, dried, and burned them at 200°C in a muffle furnace. The resulting ashes (0.3 kg at 10% yield percentage) were cooled, pulverized, and sieved to obtain a powdered substance (**Figure 1**). The concrete matrix (cement, sharp sand, and granite) was mixed with coconut shell ash powder at different percentages by weight, as shown in **Table 1**, to obtain samples A W/C ratio of 0.5 was adopted throughout the mixing procedure [27]. About 25 ml amount of water was added to each mixture; stirred, molded into discs of diameter 20 mm and height 60 mm, and allowed to dry at room temperature for a few days until constant weight was achieved. The control was mixed without the coconut shell ash at a mixing proportion by weight of 0.5 kg :1 kg :1 kg of cement, sand, and granite respectively. Other concretes were mixed with 10%, 20%, and 30% of the coconut shell ash at a mixing proportion by weight of 0.45 kg: 1 kg: 1 kg: 0.05 kg, 0.4 kg:1kg: 1kg: 0.1kg and 0.35kg: 1kg: 1kg: 0.15kg respectively of cement, sand, granite, and coconut-shell-ash respectively. The samples were further oven dried at a lower temperature of about 100 ^{o}C for two hours to remove any traces of water content left in the samples.

Table 1: Mixing Proportion of Concrete and Coconut Shell Ash (CSA)

Sample ID	Sand (kg)	Granite (kg)	Cement (kg)	CSA (kg)	WUE (%)	Density (g/cm^3)
0%CC	1.00	1.00	0.50	0.00	00.00	2.40
10%CC	1.00	1.00	0.45	0.05	16.67	2.28
20%CC	1.00	1.00	0.40	0.10	33.33	2.24
30%CC	1.00	1.00	0.35	0.15	50.00	2.20

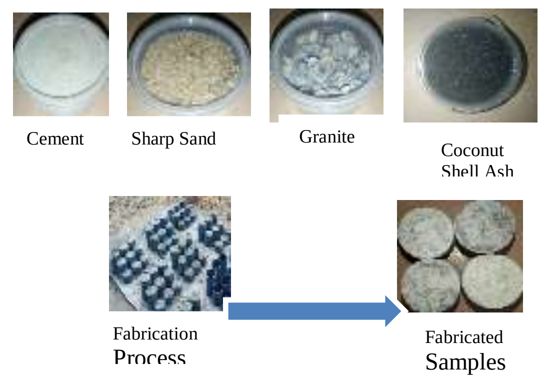

Fig. 1: Samples Fabrication Procedure.

2.3 Calculation of the Weight of Coconut Shell (WCS) Needed

The content of coconut shell ash needed to replace the cement in this work was calculated from Equation 1 as pointed out by Petrucci et al., (2017) [28], and Smith & Van-Ness (2005) [29].

$$WCS\ needed\ = \frac{Desired\ weight\ of\ coconut\ shell\ ash}{Yield\ percentage} \tag{1}$$

2.4 Measurement of Density

The fabricated concrete samples' density (ρ, g/cm^3) was measured according to the relation described in Equation 2 as reported by Rilwan et al., (2025) [30]. The total masses (M, g) of the prepared concretes were obtained using a digital balance with an accuracy of ±0.01 g. Then, the volume (V, cm^3) of prepared concrete samples was evaluated through the dimensions of the prepared samples where $V=\pi\times r^2\times h$: r and h represent the radius and the height of cylindrical shape samples.

$$\rho\ (g/cm^3) = \frac{M\ (g)}{V\ (cm^3)} \tag{2}$$

2.5 Analysis of the elemental composition

With the aid of a Thermo-Scientific X-ray fluorescence which was connected to ARLQUANT'X-EDXRF-Analyzer, with uncertainty of 1 % to 2 % and maximum energy resolution is 40 KeV, the chemical compositions of the produced concretes were identified, and quantified. The typical principle for the analysis of XRF includes weighing

2 g of each sample, placing it on a sample holder, and covering it tightly with cotton wool to prevent spraying. **Table 2** displays the obtained elemental chemical composition (wt.%) of the developed concretes (C1-C4) [31-33].

Table 2: The chemical composition of the prepared CSA concrete samples as detected by the EDXRF spectroscopy

Oxides	0%CC	10%CC	20%CC	30%CC
Fe_2O_3	1.479	1.413	1.25	0.818
SiO_2	40.775	40.677	38.473	34.473
Al_2O_3	7.734	6.816	5.341	4.847
MgO	1.53	1.68	2.16	2.27
P_2O_5	0.378	0.262	0.218	0.215
SO_3	1.228	1.031	0.946	0.941
TiO_2	0.202	0.193	0.177	0.085
MnO	0.081	0.081	0.078	0.055
CaO	23.596	19.555	18.473	16.953
K_2O	1.934	1.944	2.27	2.511
SrO	4.951	4.496	4.322	4.824
BaO	0.48	0.481	0.481	0.473

2.6 Experimental measurement of radiation shielding properties

This work utilizes NaI (sodium iodide detector) with a 24 % relative efficiency to identify gamma spectra from Co-60, and Cs-137 γ-ray sources in the energies range of 0.15-0.6 MeV. The measurements were done with the aid of a narrow beam technique, in which a lead collimator was utilized between the NaI-detector and the gamma source. **Figure 2** depicts the experimental setup of measurements of the attenuation factor, where the concrete sample was positioned at a suitable point between the gamma source and the NaI. The total count rate of the recorded gamma spectra was recorded in the presence of a concrete sample (I_x) and another in the absence of the concrete sample (I_o). The experimental linear attenuation coefficient (LAC) (μ, cm^{-1}) was determined from these values through Equation 3 [28,30,34], and the values are presented in **Table 3**.

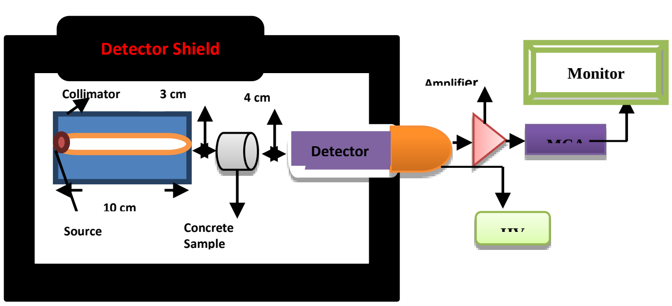

Fig. 2: Experimental setup.

$$LAC\ (cm^{-1}) = \frac{1}{x}\ln\left(\frac{I_o}{I_x}\right) \quad (3)$$

where x is the thickness of the observed concrete sample. Equations 4-9 [34] can be used to express the other relevant shielding-related parameters, such as the mass attenuation coefficient (MAC, cm^2/g), half value layer (HVL, cm), tenth value layer (TVL, cm), mean free path (MFP, cm), transmission factor (TF, %), and radiation protection efficiency (RPE, %) depending on the calculation of I_x and I_o.

$$MAC\ (cm^2/g) = \frac{LAC\ (cm^{-1})}{\rho\ (g/cm^3)} \quad (4)$$

$$HVL\ (cm) = \frac{\ln(2)}{LAC} \quad (5)$$

$$TVL\ (cm) = \frac{\ln(10)}{LAC} \quad (6)$$

$$MFP\ (cm) = \frac{1}{LAC} \quad (7)$$

$$TF\ (\%) = \frac{I_x}{I_o} \quad (8)$$

$$RPE\ (\%) = \frac{I_x}{I_o} - 1 = \frac{(I_o - I_x)}{I_o} \times 100 \quad (9)$$

In Equation 9, I_x values give the photon intensity which was noticed within the produced concrete samples. The data for LAC and MAC obtained from the experimental technique were compared with the ones obtained from the Phy-X/PSD [34] program in the energy range of 0.15-0.6 MeV. The Phy-X/PSD application can compute several radiation shielding parameters such as mass attenuation coefficient (MAC, cm^2/g), half value layer (HVL, cm), tenth value layer (TVL, cm), mean free path (MFP, cm), and linear attenuation coefficient (LAC, cm^{-1}) using the elemental compositions of the samples, obtained from EDXRF chemical composition analysis and the calculated density of the samples as an input data.

The relative deviation between the experimental and theoretical data as presented in **Table 3** was calculated using Equation 10, to ascertain the level of agreement between the experimental data and theoretical computations.

$$RD,\% = \frac{Exp\ Data - The\ Data}{The\ Data} \times 100 \quad (10)$$

Table. 3. Linear attenuation coefficient (LAC) of different concrete samples at different energies for both experimental and theoretical (Phy-X) with their respective relative deviation (RD%).

E, MeV	Method	0%CC	10%CC	20%CC	30%CC
0.15	Exp	0.386	0.354	0.348	0.377
	Phy-X	0.389	0.359	0.358	0.363
	RD%	0.771	1.393	2.793	3.857
0.2	Exp	0.333	0.304	0.309	0.301
	Phy-X	0.325	0.299	0.302	0.298
	RD%	2.462	1.672	2.318	1.007
0.3	Exp	0.275	0.250	0.255	0.248
	Phy-X	0.266	0.245	0.249	0.242
	RD%	3.383	2.041	2.410	2.479
0.4	Exp	0.241	0.225	0.228	0.218
	Phy-X	0.234	0.216	0.219	0.212
	RD%	2.991	4.167	4.110	2.830
0.5	Exp	0.215	0.201	0.205	0.197
	Phy-X	0.212	0.195	0.199	0.192
	RD%	1.415	3.077	3.015	2.604
0.6	Exp	0.189	0.175	0.178	0.169
	Phy-X	0.195	0.180	0.183	0.177
	RD%	3.077	2.778	2.732	4.520

2.7 Cost-effectiveness and waste management evaluation

As the cement is being replaced with CSA in this work, the reduction in cost (material cost saving MCS%) as well as waste utilization efficiency (WUE%) of concrete production of our concretes were computed from Equation 11 and 12 as pointed out by Kavishan et al. (2023) [35].

$$MCS,\% = \frac{Cement\ Cost - CSA\ Cost}{Cement\ Cost} \times 100 \qquad (11)$$

$$WUE,\% = \frac{CSA\ Used}{Total\ CSA\ Waste} \times 100 \qquad (12)$$

where the cost of cement at the time of this research was 10, 000 NGN per 50 kg and that of CSA was 1,000 NGN per 50 kg. The total CSA waste used as computed by Equation 1 was 300 grams (0.3 kg) and the CSA used in 0%CC, 10%CC, 20%CC, and 30%CC were respectively 0 kg, 0.05 kg, 0.1 kg, and 0.15 kg.

3 Results and Discussion

The experimental as well as theoretical MAC values for sample 0%CC were shown in **Figure 3** as a function of energy. At the lowest energy level of 0.15 MeV, the theoretical MAC shows a value of 0.162 cm^2/g which is a little higher than the experimental MAC value of 0.161 cm^2/g. As the energy increased to 0.20 MeV, the experimental MAC value became higher than the theoretical value, this trend continues up to about 0.54 MeV, indicating that the material shows a good attenuation strength within the photoelectric interaction region. As the energy increased into the Compton scattering interaction region, the theoretical MAC became higher than the experimental values, for example at 0.60 MeV, the experimental MAC showed a value of 0.079 cm^2/g while the theoretical MAC showed a value of 0.081 cm^2/g. The results of the MAC in this work agreed with the report presented by [36].

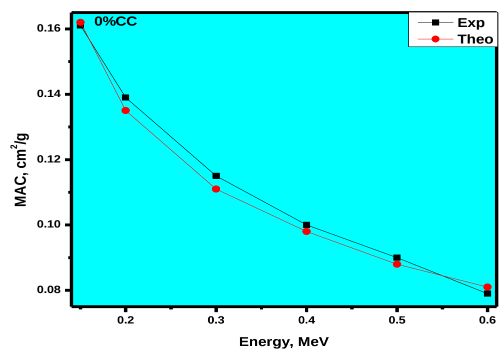

Fig. 3: A chart for the Phy-X and experimental MAC values for sample 0%CC against Energy.

The MAC for sample 10%CC as a function of the radiation's energy is shown in **Figure 4**. This figure shows both experimental and theoretical MAC for sample 10%CC. We observed that as the lowest energy level was 0.15 MeV, the Phy-X MAC value was 0.157 cm^2/g while the experimental value was 0.155 cm^2/g, this shows that the actual attenuation strength of the material at this energy level is a little less than expected which might be due to some experimental errors. As we move deeper into the photoelectric interaction region (from 0.20 – 0.54 MeV), the theoretical MAC was below the values found experimentally. The trend returned to its original path at 0.60 MeV with the theoretical MAC value (0.079 cm^2/g) being higher than the experimental value (0.077 cm^2/g). This means that within the Compton scattering interaction region, the sample loses some of its shielding strength. The results of the MAC in this work agreed with the report presented by [37].

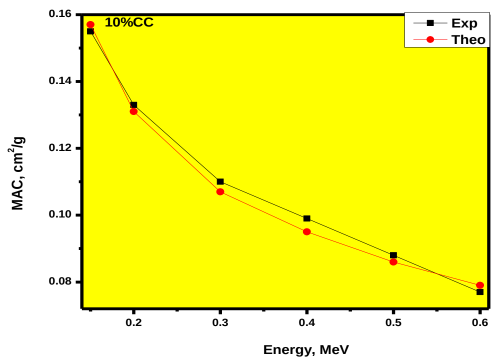

Fig. 4: A chart for the Phy-X and experimental MAC values for sample 10%CC against Energy.

At the lowest energy level considered in this research, that is 0.15 MeV, we observed that the MAC value for sample 20%CC found experimentally (0.155 cm^2/g) is a bit lower than the theoretical value (0.160 cm^2/g) found using Phy-X. as the energy increased to 0.20 MeV, the theoretical MAC value dropped lower than the experimental value, and this trend continued up to about 0.54 MeV, indicating that experimentally, the material possess good attenuation ability within the photoelectric interaction region. Increasing the energy to 0.60 MeV venturing into the Compton scattering interaction region, the attenuation strength of the material dropped a little as shown by the experimental MAC value (0.079 cm^2/g) against the theoretical MAC value (0.082 cm^2/g) **(see Figure 5).** The results of the MAC in this work agreed with the report presented by [38].

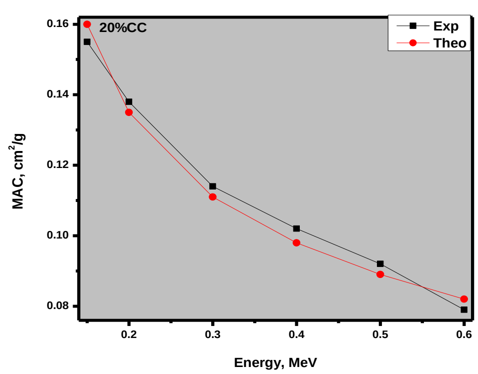

Fig. 5: A chart for the Phy-X and experimental MAC values for sample 20%CC against Energy.

The MAC calculated using Phy-X was higher than the experimental MAC value found at 0.15 MeV as shown in **Figure 6**. The theoretical MAC shows a value of 0.182 cm^2/g while the experimental MAC shows a value of 0.189 cm^2/g. The highest MAC shown by sample 30%CC both theoretical and experimental as compared to the other three samples was due to its less content of high-Z atoms in its chemical composition. As the energy increased to 0.20 MeV, the MAC values dropped significantly with the experimental MAC showing a value of 0.150 cm^2/g while the theoretical MAC shows a value of 0.149 cm^2/g. Further increase in the energy within the photoelectric interaction region (0.20 – 0.54 MeV) shows a continuous decrease in the MACs with theoretical values consistently being below the experimental value indicating that the material has a better attenuating ability practically than the simulated version. At the highest energy level considered in this research (0.60 MeV), the theoretical value (0.089 cm^2/g) became higher than the experimental value (0.085 cm^2/g) showing that the material loses some of its shielding ability at the Compton scattering interaction region. The results of the MAC in this work agreed with the report presented by [38].

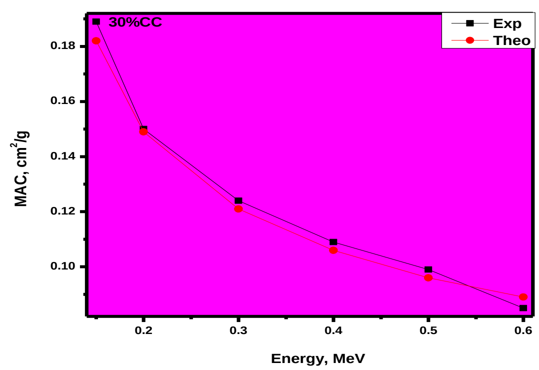

Fig. 6: A chart for the Phy-X and experimental MAC values for sample 30%CC against Energy.

Based on the computed RD (relative deviation), significant variation was observed between the experimental and theoretical data, with varieties of percentage compositions of concrete (CC%) as shown in **Figure 7**. The deviations were observed to be great at lower energy range, with values ranging between 0.771% to 3.857% for concrete samples 0%CC to 30%CC. At enhanced energy of 0.2 MeV, a sudden increase was observed up to 2.462% in the 0%CC sample, and a fast fall up to 1.007% was noticed in the concrete sample 30%CC, which showed that there is an improved agreement between experimental and theoretical data. When the energy increased to 0.5 MeV, the values ranged from 1.415% and 3.015%, which confirmed that the compositions are consistent. It was interestingly noted that concrete sample 30%CC had a superior deviation of 4.520%, unlike the remaining concrete samples which showed minimal fluctuations. The entire order confirmed that, at a higher energy range, more agreement was observed between experimental and theoretical data, especially in the less %CC mixes. The results of the MAC in this work agreed with the report presented by [39].

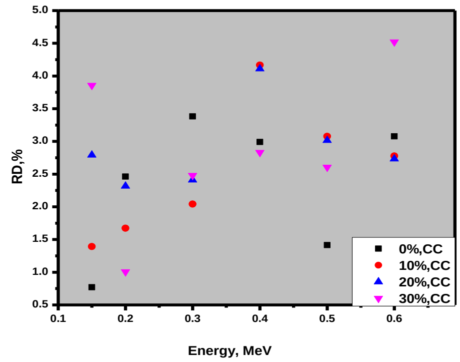

Fig. 7: Plot of RD% versus gamma energy.

At the lowest energy level considered in this study (0.15 MeV), sample 0%CC shows the highest LAC (0.386 cm^{-1}) among the studied samples, followed by sample 10%CC with a LAC value of 0.377 cm^{-1} as in **Figure 8**. This highest LAC shown by sample 0%CC was due to its chemical composition content of higher atomic number oxides such as Fe_2O_3, SiO_2, and TiO_2 giving it a stronger attenuation capability. As the energy increased from 0.15 – 0.60 MeV, we noticed a drastic decrease in the LAC values for all the samples, with sample 0%CC consistently showing higher LACs as shown in figure 8, for example, at 0.60 MeV the LAC value shown by sample 0%CC was 0.189 cm^{-1}, while sample 30%CC shows the lowest LAC value (0.169 cm^{-1}) at this energy level. All other sample's LAC falls in between these extreme values. Hence sample 0%CC has the highest shielding ability at all energy levels considered. The results of the MAC in this work agreed with the report presented by [39].

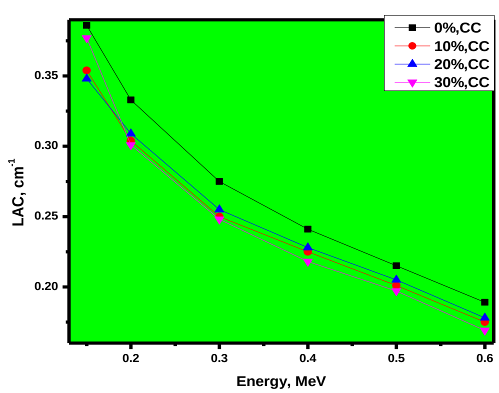

Fig. 8: A chart of the Linear Attenuation Coefficient LAC against Energy E (in MeV) for all the studied concretes.

The sample thickness needed to shield 50% of the incoming radiation for all the samples at different energy levels is shown in **Figure 9**. At the lowest energy level considered (0.15 MeV), all the samples show lower HVLs with sample 0%CC having the least HVL at this energy level; the HVL shown by sample 0%CC was 1.780 cm, followed by sample 30%CC with HVL value of 1.840 cm, sample 10%CC shows HVL value of 1.958 cm, while sample 20%CC shows the highest LAC at this energy with a value of 1.990 cm. As the energy increased from 0.15 to 0.60 MeV, the HVLs increased significantly with sample 0%CC consistently showing the lowest HVL while sample 30%CC shows the highest HVL except at 0.15 MeV. For example, at 0.60 MeV sample 0%CC shows an HVL value of 3.667 cm while sample 30%CC shows an HVL value of 4.100 cm. This lower HVLs shown by sample 0%CC indicates its highest attenuating ability among the other fabricated samples. The results of the MAC in this work agreed with the report presented by [39].

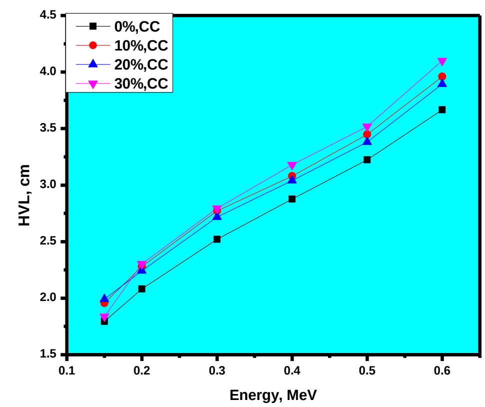

Fig. 9: A chart of the Half Value Layer HVL against the Energy of the radiation (in MeV) for all the concrete samples.

The tenth value layer (TVL) for all the samples at different energy levels was plotted as shown in **Figure 10**. Sample 0%CC shows the lowest TVL (5.966 cm) at the lowest energy level considered (0.15 MeV) followed by sample 30%CC with a TVL value of 6.109 cm, while sample 20%CC shows the highest TVL at this energy level. As the energy increased from 0.15 to 0.60 MeV, the TVLs also increased rapidly with sample 0%CC consistently showing the lowest TVL while sample 30%CC shows the highest TVL except at 0.15 MeV. The high TVL shown by sample 0%CC was due to its high content of high-Z atoms in its chemical composition which increased the interaction between the molecules of the sample and the radiation. As an illustration, sample 0%CC shows TVL value of 12.185 cm at 0.60 MeV while sample 30%CC shows TVL value of 13.627 cm. This indicates that sample 0%CC has the highest attenuating ability among the other fabricated samples. The results of the MAC in this work agreed with the report presented by [40].

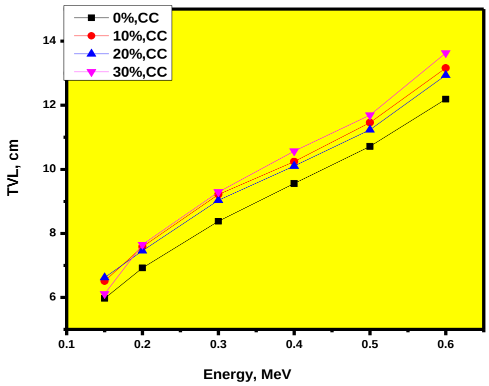

Fig. 10: A chart of the Tenth Value Layer TVL against the Energy of the radiation (in MeV) for all the concrete samples.

The average distance traveled by the radiation before interacting with the concrete molecules was plotted against the energy of the incoming radiation as shown in **Figure 11**. At the lowest energy level of 0.15 MeV, the MFP shown by sample 0%CC was the lowest with a value of 2.591 cm, followed by sample 30%CC with an MFP value of 2.653 cm, sample 10%CC shows an MFP value of 2.824 cm, while sample 20%CC shows the highest MFP with a value of 2.874 cm. As the energy increased from 0.15 – 0.60 MeV, we observed an incredible increase in the MFPs across all the fabricated samples. At the highest energy level of 0.60 MeV, sample 0%CC also shows the lowest MFP with a value of 5.291 cm while sample 30%CC shows the highest MFP with a value of 5.917 cm, other samples have MFPs in between these extreme values. The lowest MFPs shown consistently by sample 0%CC was due to its content of higher atomic oxides in its chemical composition making it the best radiation shielding material among the fabricated samples. The results of the MAC in this work agreed with the report presented by [40].

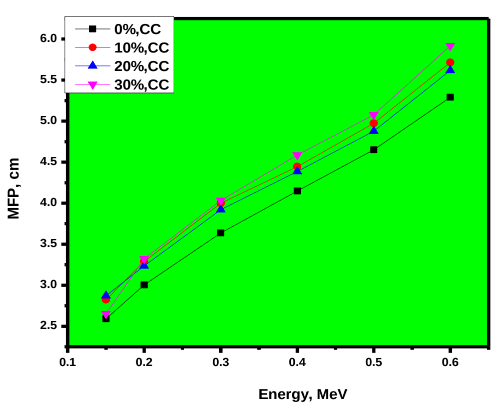

Fig.11: A chart of the Mean Free Path MFP against Energy of the radiation (in MeV) for all the concrete samples.

At the lowest energy level considered in this research (0.15 MeV), we observe a small transmission value for the radiation in all the studied samples. For example, sample 0%CC shows the lowest TF value at this energy level with a value of 0.099, followed by sample 30%CC with a TF value of 0.104, and sample 10%CC and 20%CC show an equal TF value (0.120). Increasing the energy from 0.15 – 0.60 MeV, we observe a significant increase in all the TFs shown by the studied samples **(see Figure 12)**. For example, at 0.60 MeV, sample 30%CC shows the highest TF value (0.363) due to its lowest content of the high-Z oxides in its chemical composition, making it the poorest radiation shielding material, while sample 0%CC consistently shows the lowest TF values (0.322) indicating the highest radiation shielding capability. The results of the MAC in this work agreed with the report presented by [41].

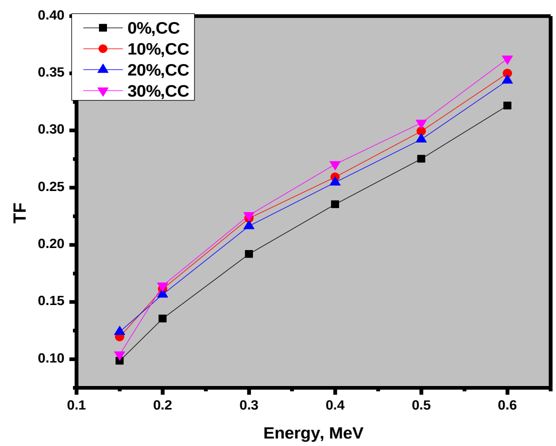

Fig. 12: A chart of the Transmission Factor TF against Energy of the radiation (in MeV) for all the concrete samples.

The radiation protection efficiency shown by sample 0%CC was the highest at the lowest energy value of 0.15 MeV with a value of 0.901%, followed by sample 30%CC with an RPE value of 0.896%, sample 10%CC shows an RPE value of 0.880%, while sample 20%CC shows an RPE value of 0.876%. As the energy increases as shown in **Figure 13**, we noticed a rapid decrease in all the RPE values shown by the studied samples. For example, at the highest energy level (0.60 MeV) sample 0%CC shows an RPE value of 0.678% which happens to be the highest at this energy level, while sample 30%CC shows the lowest RPE with a value of 0.637%. The highest RPEs shown by sample 0%CC were due to its high content of oxides with higher atomic numbers such as Fe_2O_3, SiO_2, and TiO_2 which increases its attenuating ability; hence, sample 0%CC became the best radiation shielding material. The results of the MAC in this work agreed with the report presented by [41].

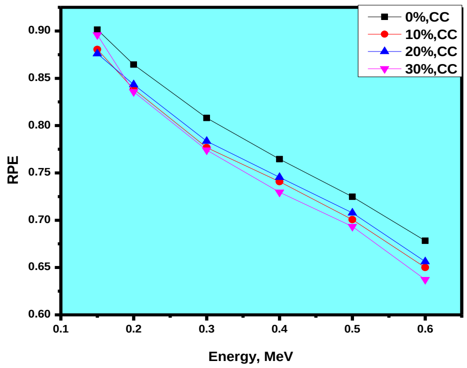

Fig. 13: A chart of the Radiation Transmission Efficiency RPE against Energy of the radiation (in MeV) for all the concrete samples.

Figure 14 shows the plot of waste utilization efficiency against coconut shell ash (CSA) content. In the plot, it was shown that the concrete sample with 0% CSA has the least value of WUE (0%) followed by the concrete sample with 10% CSA, which has a WUE value of 16.67%, then the concrete sample with 20% CSA, with WUE value up to 33.33%, and lastly, the concrete sample with 30% CSA had the highest value of WUE up to 50%. The material cost saving (MCS) in this work was calculated from Equation 11 and 90% MCS was recorded. These results indicated that, economically and environmentally, the utilization of CSA as a partial replacement of cement enhances sustainable management of waste and reduces the cost of materials. The results of the MAC in this work agreed with the report presented by [42].

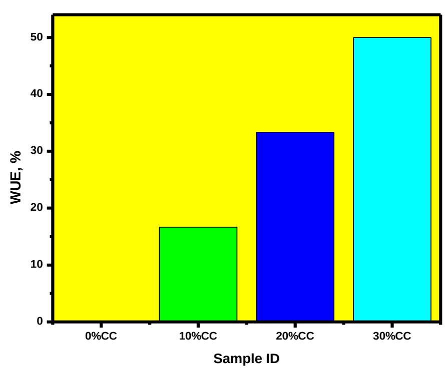

Fig.14: Waste Utilization Efficiency (WUE) against Coconut Shell Ash (CSA) Content.

4 Conclusions

In this study, we partially replaced cement with coconut shell ash (CSA) to produce four new concretes and tested the effects of the CSA on the new concrete's gamma-ray shielding efficiency, cost-effectiveness, and environmental sustainability. The results for both the theoretical and the experimental linear attenuation coefficient (LAC) of 0%CC showed a high value (0.386 cm^{-1}) at a lower energy range (0.15 MeV). Higher attenuation was observed also at lower energies when the CSA was added to the concrete matrix (30%CC). 2.591 cm MFP (mean free path) was observed at a lower energy level of 0.15 MeV, which implied high shielding ability. 50% waste utilization efficiency (WUE) was achieved for sample 30%CC with total material cost savings (MCS) of about 90%. Validation of experimental results with Phy-X simulation software revealed that RD (relative deviation) falls between 0.771% to 4.520%, confirming the validity of the experimental results. The incorporation of CSA does not enhance the shielding ability alone but further minimizes the environmental implications through reduction of the emission of carbon which is related to the production of cement. The study showed that CSA is a good replacement for conventional shielding concretes produced from cement, strongly agreeing with the SDGs (sustainable development goals), and also giving insight into the utilization of agricultural wastes in concretes to ensure radiation shielding in hospitals and other fields where radiation is applied. Other authors can focus on the long-term durability and multi-functional utilizations of CSA-based concretes in various environments.

Acknowledgment

The authors thankfully acknowledge the staff of the Physics Department, Nigerian Army University, Biu, and the staff of the Physics Department, Abubakar Tafawa Balewa University, Bauchi for their support and positive criticism throughout the development of this research paper.

References

[1] Abdullahi, S. L., and Audu, A. A. Comparative analysis on the chemical composition of bentonite clays obtained from Ashaka and tango deposits in Gombe State, Nigeria. *Chem Search Journal*, **8(2)**, 35–40, (2017.

[2] Rehab M El-Sharkawy, Elhassan A Allam, Atef El-Taher, Reda Elsaman, E El Sayed Massoud, Mohamed E Mahmoud, Synergistic effects on gamma-ray shielding by novel light-weight nanocomposite materials of bentonite containing nano Bi2O3 additive. *Ceramics International* 48 (5), 7291-7303.2022.

[3] Rehab M El-Sharkawy, Elhassan A Allam, Atef El-Taher, Mahmoud, ME., Synergistic effect of nano-bentonite and nanocadmium oxide doping concentrations on assembly, characterization, and enhanced gamma-rays shielding properties of polypropylene. International *Journal of Energy Research* 45 (6), 8942-8959.2021.

[4] Adegbulugbe Samuel Kanmi, Umar Ibrahim, N.G. Goki, U. Rilwan, M.I. Sayyed, Yasser Maghrbi, Berivan F. Namq, Laith Ahmed Najam, Taha Yaseen Wais, Assessment of natural radioactivity and its radiological risks in the soil of local government areas (Asa, Ilorin East, Ilorin South, Irepodun, Moro, and Oyun) in Kwara State, Nigeria, *Case Studies in Chemical and Environmental Engineering*, **101040**, 2024. https://doi.org/10.1016/j.cscee.2024.101040.

[5] ALHASSAN, M; BARAYA, J. T; GARBA, A. S. Accuracy of Phy-X/PSD Software Compared to XCOM in the Determination of Mass Attenuation Coefficient of Glass Systems. J. Appl. Sci. Environ. Manage. **27(5)** 985-988, 2023. https://dx.doi.org/10.4314/jasem.v27i5.15

[6] Aljawhara H. Almuqrin, K.A. Mahmoud, U. Rilwan, M.I. Sayyed, Influence of various metal oxides (PbO, Fe2O3, MgO, and Al2O3) on the mechanical properties and γ-ray attenuation performance of zinc barium borate glasses, Nuclear Engineering and Technology, **56(7)**, 2711-2717, 2024. https://doi.org/10.1016/j.net.2024.02.032.

[7] Aljawhara H. Almuqrin, M.I. Sayyed, Ashok Kumar, U. Rilwan, Characterization of glasses composed of PbO, ZnO, MgO, and B2O3 in terms of their structural, optical, and gamma-ray shielding properties, Nuclear Engineering and Technology, 56(7), 2842-2849, 2024. https://doi.org/10.1016/j.net.2024.02.047.

[8] Turner, J.E. *Atoms, Radiation and Radiation Protection*, third ed., John Wiley and Sons, New York, 5227-5230, 2017.

[9] Chen, X., Zhang, D., Liu, W., & Liu, Y. Performance of high-density concrete with different aggregates for radiation shielding. *Construction and Building Materials*, **162**, 171-180, 2018.

[10] El-Sharkawy, RM., Allam, EA., El-Taher, A., Shaaban, ER., Mahmoud, ME., Synergistic effect of nano-bentonite and nanocadmium oxide doping concentrations on assembly, characterization, and enhanced gamma-rays shielding properties of polypropylene. International *Journal of Energy Research* 45 (6), 8942-8959.2021.

[11] Allam, EA., El-Sharkawy, RM., Shaaban, Kh S., El-Taher, A. Mahmoud, ME., El Sayed, Y., Structural and thermal properties of nickel oxide nanoparticles doped cadmium zinc borate glasses: preparation and characterization. Digest *Journal of Nanomaterials & Biostructures* (DJNB) 17 (1).2022.

[12] El-Sayed, A. K., El-Esrity, B. S., & Abbas, H. H. Improving the radiation attenuation properties of cement-based composites using diatomite and barite minerals. *Construction and Building Materials*, **199**, 219-228, 2019.

[13] Heba Jamal Alasali, U. Rilwan, K.A. Mahmoud, Taha A. Hanafy, M.I. Sayyed, Comparative analysis of TiO2, Fe2O3, CaO and CuO in borate-based glasses for gamma ray shielding, Nuclear Engineering and Technology, **56(10)**, 4050-4055, 2024. https://doi.org/10.1016/j.net.2024.05.006.

[14] Negm, HH., Allam, EA., Abdeltwab, E., Mostafa, M., Mahmoud, ME and El-Taher, A., A new nanocomposite of copper oxide and magnetite intercalated into Attapulgite clay to enhance the radiation shielding. *Radiation Physics and Chemistry* 216, 111398.2024.

[15] Hosseini, S. A., Ghofrani, M. B., & Mollahosseini, A. Effects of various aggregates on radiation attenuation properties of concrete. *Journal of Structural and Construction Engineering*, **4(1)**, 1-7, 2017.

[16] Hosseini, S. A., Ghofrani, M. B., & Mollahosseini, A. Effects of various aggregates on radiation attenuation properties of concrete. *Journal of Structural and Construction Engineering*, **4(1)**, 1-7, 2017.

[17] Taqi, A. H. & Khalil, H. J. Experimental and theoretical investigation of gamma attenuation of building materials, *J. Nucl. Particle Phys*. **7(1)**, 6-13, 2017.

[18] Kim, J. D., Ahn, S., Lee, Y. D., and Park, C. J. Design optimization of radiation shielding structure for lead slowing-down spectrometer system. *Nuclear Engineering and Technology*, **47(3)**, 380–387, 2015.

[19] Knoll, G.F. *Radiation Detection and Measurement*, third ed., John Wiley and Sons, New York, 222-225, 2000.

[20] M. I. Sayyed, Aljawhara H. Almuqrin, Chaitali V. More, U. Rilwan, M. Rashad, Mohamed Elsafi. Exploring Gamma Radiation Shielding: the Role of BaO in Borosilicate Glasses. *Silicon* **16**, 4857–4866, 2024. https://doi.org/10.1007/s12633-024-03045-1

[21] Sayyed, M.I. & Elhouichet, H. Variation of energy absorption and exposure buildup factors with incident photon energy and penetration depth for borotellurite (B2O3-TeO2) glasses, *Radiat. Phys. Chem*. **130**, 335-342, 2017.

[22] McAlister, D. *Gamma Ray Attenuation Properties of Common Shielding Materials*, University Lane Lisle, USA, 152-157, 2012.

[23] Elhassan A Allam, Rehab M El-Sharkawy, Atef El-Taher, ER Shaaban, E El Sayed Massoud, Mohamed E Mahmoud., Enhancement and optimization of gamma radiation shielding by doped nano HgO into nanoscale bentonite. *Nuclear Engineering and Technology* 54 (6), 2253-2261.2022.

[24] Olukotun, S. F., Gbenu, S. T., Ibitoye, F. I., Oladejo, O. F., Shittu, H. O., Fasasi, M. K., and Balogun, F. A. Investigation of gamma radiation shielding capability of two clay materials. *Nuclear Engineering and Technology*, **50(6)**, 957–962, 2018.

[25] Olukotun, S. F., Mann, K. S., Gbenu, S. T., Ibitoye, F. I., Oladejo, O. F., Joshi, A., Tekin, H. O., Sayyed, M. I., Fasasi, M. K., Balogun, F. A. and Korkut, T. Neutron-shielding behavior investigations of some clay-materials. *Nuclear Engineering and Technology*, **51(5)**, 1444–1450, 2019.

[26] Olukotun, S.F., Gbenu, S.T., Oladejo, O.F., Balogun, F.O., Sayyed, M.I., Tajudin, S.M., Obiajunwa, E.I., Fasasi, M.K., (2021). The Effect of Incorporated Recycled Low-Density Polyethylene (LDPE) on the Fast Neutron Shielding Behaviour (FNSB) of Clay Matrix using MCNP and PHITS Monte Carlo Codes, *Journal of Radiation Physics and Chemistry*, 182, 109351 – 109357.

[27] U. Rilwan, G.M. Aliyu, S.F. Olukotun, M.M. Idris, A.A. Mundi, S. Bello, I. Umar, A. El-Taher, K.A. Mahmoud, M.I. Sayyed, Recycling and characterization of bone incorporated with concrete for gamma-radiation shielding applications, Nuclear Engineering and Technology, 56(7), 2828-2834, 2024. https://doi.org/10.1016/j.net.2024.02.045.

[28] R.H. Petrucci, F.G. Herring, J.D. Madura. General Chemistry: Principles and Modern Applications (11th Ed.), Pearson, 2024.

[29] J.M. Smith, H.C. Van-Ness. Introduction to Chemical Engineering Thermodynamics (7th Ed.), McGraw-Hill, 2005.

[30] U. Rilwan, S.A. Edeh, M.M. Idris, I.I. Fatima, S.F. Olukotun, G.Z. Arinseh, P.Z. Bonat, A. El-Taher, K.A. Mahmoud, Taha.A. Hanafy, M.I. Sayyed, Influence of waste glass on the gamma-ray shielding performance of concrete, Ann Nucl Energy **210** 110876, 2025. https://doi.org/10.1016/j.anucene.2024.110876.

[31] Sokol, H., Sprynskyy, M., Ganzyuk, A., Raks, V., & Buszewski, B. Structural, Mineral and Elemental Composition Features of Iron-Rich Saponite Clay from Tashkiv Deposit (Ukraine). *Colloids and Interfaces*, **3(1)**, 1–12, 2019.

[32] Sayyed, M.I., Celikbilek, E., Ersundu, A.E.E., Lakshminarayana, G. & Kostka, P. Investigation of radiation shielding properties for MeO-PbCl2-TeO2 (MeO = Bi2O3, MoO3, Sb2O3, WO3, ZnO) glasses. *Radiat. Phys. Chem*. **144**, 419-425, 2018.

[33] Scimeca, M., Bischetti, S., Lamsira, H. K., Bonfiglio, R., & Bonanno, E. (2018). Energy dispersive X-ray (EDX) microanalysis: A powerful tool in biomedical research and diagnosis. *European Journal of Histochemistry*, **62(1)**, 89–99, 2018. https://doi.org/10.4081/ejh.2018.2841

[34] El-Taher, A., HM Mahmoud, AGE Abbady., Comparative study of attenuation and scattering of gamma-rays through two intermediate rocks. *Indian Journal of Pure and Applied Physics* 45, 198-203.2007.

[35] Kavishan Sathsara Ranatunga, Enrique del Rey Castillo, Charlotte Louise Toma, Evaluation of the optimal concrete mix design with coconut shell ash as a partial cement replacement, Construction and Building Materials, 401, 132978, 2023. https://doi.org/10.1016/j.conbuildmat.2023.132978.

[36] Alshami, A. M., Al-Hadidy, A. I., Al-Ghalib, N. A., & Al-Taie, S. H. Experimental study on the effect of different weights of barite on radiation attenuation of concrete for radioactive sources shielding. *Journal of Radiation Research and Applied Sciences*, **11(3)**, 281-286, 2018.

[37] M.I. Sayyed, U. Rilwan, K.A. Mahmoud, Mohamed Elsafi, Experimental study of the radiation shielding characteristics of new PbO– Na2O–B2O3–BaO glasses, Nuclear Engineering and Technology, **56(7)**, 2437-2443, 2024. https://doi.org/10.1016/j.net.2024.01.058.

[38] M.I. Sayyed, Aljawhara H. Almuqrin, Mohamed Elsafi, U. Rilwan, Evaluation of incorporation of granite waste and SnO2-NPs into coating mortar for gamma-ray shielding, Radiation Physics and Chemistry, **222**, 111818, 2024. https://doi.org/10.1016/j.radphyschem.2024.111818.

[39] Tajudin, S.M., Sabri, A.H.A., Abdul Aziz, M.Z., Olukotun, S.F., Ojo, B.M. & Fasasi, M.K. Feasibility of clay-shielding material for low-energy photons

(Gamma/X). *Nuclear Engineering and Technology*, **51(1)**, 1633-1637, 2019.

[40] Velmathi, G. A review on morphological, structural and electrical characterization techniques of thin films. *International Journal of Engineering and Technology*, **8(5)**, 1925–1935, 2016. https://doi.org/10.21817/ijet/2016/v8i5/160805410

[41] Yahaya, S., Jikan, S. S., Badarulzaman, N. A., & Adamu, A. D. Effects of Acid Treatment on the SEM-EDX Characteristics of Kaolin Clay. *Path of Science*, **3(9)**, 4001–4005, 2017.

[42] Ahmed Khalil, Ibrahim I Bondouk, Elhassan A Allam, Islam M Nabil, Mogahed Al-Abyad, Heba Saudi, Atef El-Taher, Mohamed E Mahmoud, Ahmed Amar., A binary composite material of nano polyaniline intercalated with nano-Fe2O3 for enhancing gamma-radiation-shielding properties: experimental and simulation study. *Progress in Nuclear Energy*, 169, 105067. 2024.